A comparative study on Aluminum-Silicon coatings fabricated by ElectroSpark Deposition

G. Renna, P. Leo

In today's industrial sector, there is a growing interest in eco-friendly practices, along with the essential goal of improving the durability and resistance to wear and corrosion of mechanical components exposed to harsh environments by applying coatings. A key technology meeting these objectives is Electrospark Deposition (ESD), a micro-welding process that allows electrically conductive substrates to be coated with different materials. ESD also facilitates precise, small-scale repairs of high-value components damaged, worn, or affected by manufacturing defects.
This study examines and compares the quality of A357 and C355 aluminium alloy coatings deposited on homologous substrates using ESD technology. It focuses on microstructural characteristics, mechanical properties, and stereological features.
Three different discharge power levels were used to deposit coatings on both aluminium alloys. The cross-sectional coatings were examined using scanning electron and optical microscopy to analyse their microstructure and evaluate the coating quality in detail. Additionally, the mechanical properties of the coatings were assessed through Vickers microhardness testing.
The microstructural analysis indicates that irrespective of the discharge power employed, all coatings exhibit a very fine microstructural morphology attributed to rapid solidification. Furthermore, experimental findings reveal that all coatings exhibit defects, manifested in the form of various morphologies of voids. Additionally, unlike the A357 sample, the C355 samples display cracks at the interface between the substrate/coating, extending into the base material. The defects percentage within the A357 and C355 coatings, primarily attributed to mass transport and stress thermal, is less than 4 and 8%, respectively. Finally, microhardness values in all coatings, irrespective of discharge power settings, are lower than the substrate material. This is primarily attributed to the presence of internal defects.

KEYWORDS: ALUMINIUM ALLOYS, ELECTROSPARK DEPOSITION (ESD), MICROSTRUCTURE, COATINGS, C355 ALLOY, A357 ALLOY

INTRODUCTION

In the aeronautical and automotive industries, the current trend to address fuel consumption and weight reduction issues is to use light metal alloys to produce various components as an alternative to traditional iron-based alloy components. Aluminium cast alloys are the preferred choice for these fields due to their good castability, strong corrosion resistance, and high strength-to-weight ratio [1,2]. Additionally, these alloys benefit from heat treatment, further enhancing their properties. At the industrial level, the most used Al alloys are A357 (belonging to the AlSi7Mg system) and C355 alloy (quaternary Al–Si–Cu–Mg alloy) which are usually processed by low-pressure die-casting and

Gilda Renna, Paola Leo
Department of Engineering for Innovation,
University of Salento, Lecce

gilda.renna@unisalento.it

gravity semi-permanent mold technology [3,4]. The A357 alloy properties depend on the distribution of the Mg and Si alloying elements in the Al matrix and the Mg2Si second-phase precipitates [5]. In the automotive field, it has found a variety of uses over the years to produce engine blocks such as cylinder heads, pistons, and brake callipers, while in aerospace have been made engine mounts in fighter planes and ailerons [6-8]. Instead, due to their high strength at high temperatures, the C355 alloy is found in the aircraft and automotive industry in the form of aircraft supercharger covers, fuel-pomp bodies, air-compressor pistons, liquid-cooled aircraft engine crankcases, motor mounts, cylinder heads, heat exchangers, air conditioners, transmissions housings, wheels, fenders, loads floor and suspension components [9]. In general, during solidification, different intermetallic phases can form in an Al-Si-Cu-Mg aluminium alloy (i.e C355 alloy), depending on its overall composition. The chemical composition, relative fraction volume and shape (morphology) of these phases significantly influence the alloy's technological properties. However, to improve the mechanical properties and ductility, both alloys are generally heat-treated. The heat treatment consists of solution treatment, quenching and artificial ageing. After solution treatment and quenching, the Mg and Cu-rich intermetallic compounds dissolve into the Al matrix [9-12].

Generally, the mechanical components made with these alloys during their service life are subject to wear resulting from prolonged use and exposure to aggressive environments. Therefore, another challenge at an industrial level is to reduce the costs related to the replacement of damaged components. On the other hand, it is known that a large fraction of maintenance costs is due to the disassembly and transport of components where on-site repair is not possible. For these reasons, researchers and industries are placing a high level of attention on the development of innovative, low-cost and eco-friendly processes for restoring damaged or worn components, which allow such repairs to be carried out directly in loco [13,14].

Nowadays, one of the processes able to satisfy the above-mentioned requirements is the Electrospark Deposition (ESD). This is a micro-welding process used in the small-scale precision repair of high-value components that are damaged, worn, or have manufacturing defects. Moreover, it also be used as a coating technique for electrically conductive substrates by depositing materials that are homologous or dissimilar to the substrate, to improve the surface mechanical or chemical properties of the substrate. In addition to the small size of the equipment, one of the advantages that distinguishes it from other traditional repair processes is the reduced heat input induced in the substrate. Several researches show that the ESD process can originate an excellent metallurgical bond between the substrate and the coating, thanks to the metallurgical reaction as fusion and diffusion, without inducing changes in the microstructure of the substrate [14,15].

To date in the literature, studies on the possibility of using this process as a repair or coating technique are mainly aimed at steel alloys and superalloys [16-18], leaving ample space for in-depth analysis on the possible uses of this process for light alloys, such as aluminium.

Therefore, this work aims to evaluate the feasibility of using ESD as a deposition technique of A357 and C355 aluminium alloy on substrates of the same material. Attention was paid to the influence of the power used on the deposition efficiency in terms of identifying the criticalities associated with the ESD of aluminium alloys given a possible application of this process as a repair of components in the aeronautical field. Furthermore, the microstructure and mechanical properties of the obtained coatings were also evaluated. This comprehensive exploration sheds light on the intricate interplay between discharge power, alloy composition and coating characteristics in the context of ElectroSpark Deposition technology.

MATERIALS AND EXPERIMENTAL PROCEDURES

This study was conducted on two different casting Al alloys: A357 and C355 alloy. Both Al alloy substrate was supplied in T61 condition (solution heat treated at 540°C for 18 h, quenched in water at 20 to 30°C, aged at 200°C for 7 h) as discs 30 mm in diameter and 5 mm thick. Their chemical compositions are shown in Table 4.1.

Tab.1 - Chemical composition (%wt) of the A357 and C355 alloy.

	Cu	Si	Mn	Mg	Zn	Ti	Fe	Others	Al
A357	<0,05	6,5-7,5	<0,03	0,45-0,6	0,05	<0,2	0,15	<0,15	Bal.
C355	1,3	5	0,1	0,5	-	0,1	0,2	0,15	Bal.

The ESD machine used to fabricate the depositions was the "TechnoCoat Micro Depo Model 150". The coatings were performed manually at room temperature by moving the electrode along the same line and carrying out 50 consecutive passes. Cylindrical rods, with the same composition as the substrate, 2.3 mm in diameter and approximately 50 mm in length were used as electrodes (anodes). The electrodes were manufactured without specifications. They are made by casting in bars, solubilization and wire drawing.

Before the depositions, the substrate was previously smoothed with 800-grit SiC paper. During the depositions, the rotation speed of the electrode was kept constant and equal to ~1200 rpm, whereas the other three main parameters were properly varied: voltage, capacitance, and frequency. All the depositions were performed in the presence of a constant flow of Argon equal to 17 L/min.

Three different levels of discharge power were used to make the A357 and C355 aluminum alloy coatings. Tables 1 and 2 summarize the parameters used for each of the two alloys studied. Particularly, the discharge power of the process was calculated as:

$$P = \frac{1}{2} C V^2 f$$

where V is the capacitor charge voltage in Volts (V), C is the capacitance in micro-Farads (μF), and f is the capacitor discharge frequency in hertz (Hz).

Tab.2 - ESD process parameters used for the A357 depositions. The shielding gas flow rate was 17 l/min.

Samples	Voltage [V]	Capacitance [μF]	Frequency [Hz]	P [W]
A1	100	100	66	33
A2	100	150	66	49,5
A3	100	100	280	140

Tab.3 - ESD process parameters used for the C355 depositions. The shielding gas flow rate was 17 l/min

Samples	Voltage [V]	Capacitance [μF]	Frequency [Hz]	P [W]
C1	100	50	148	37
C2	150	80	148	133,2
C3	150	50	390	219,4

After coatings deposition, the samples obtained were cut orthogonally to the direction of the electrode feed, embedded, and prepared for metallographic observation. Cross sections were etched using Keller reagent (95 mL H_2O, 2.5 mL HNO_3, 1.5 mL HCl, 1 mL HF). Microstructural analysis was conducted using an optical microscope (Nikon Model Epiphot 200) and a scanning electron microscope (Zeiss Evo) equipped with an energy dispersive spectrometer (EDS). To characterize both the morphology of the coatings and the defects present, the NIS Element AR image analysis software, supplied with the optical microscope, was used.

The micro-hardness was performed in the coating cross-section with a Vickers hardness tester by applying a load

equal to 100 gr for a dwell time of 15 s ($HV_{0.1/15}$). In particular, the micro-hardness of both the coatings and the base material was evaluated by performing six indentations at a distance of 100 μm from the substrate/coating interface. The measurements were performed in accordance with the reference standard ASTM E-384.

The average thickness of each coating was evaluated by performing an average of five measurements taken respectively at the center of the substrate-deposit interface and 250 μm and 500 μm from it.

RESULTS AND DISCUSSION

Base Material Microstructure

Figure 1a-f shows optical and scanning electron micrographs (SEM) of the as-received A357-T61 and C355-T61 alloy substrates. The microstructure of these alloys, which are characterized by a silicon content of less than 12.6 wt% (hypoeutectic alloys), consists of α-Al dendrites, the eutectic Si phase, and various secondary intermetallic phases (Fig. 1a,d) [19,20]. Intermetallic phases, found in interdendritic regions and along grain boundaries, contain iron (Fe), magnesium (Mg), copper (Cu), manganese (Mn) and silicon (Si). The fraction, size, morphology, and composition of these phases, which are formed during the solidification process, depend on the chemical composition of the alloy and the solidification rate (solidification conditions) [9,21]. Based on the literature and phase morphology [9,21-23], the A357-T61 microstructure consists mainly of small spherical Si particles (dark grey particles), Mg_2Si particles, together with intermetallic π-(Al8Mg3FeSi6) phase, and a small number of α-Al_5FeSi phase (Fig 1b,c). In contrast, the C355-T61 substrate exhibits a coarser microstructure due to its higher levels of copper (Cu) and manganese (Mn). Specifically, it can be observed coarse polyhedric Si particles and the presence of other new intermetallic phases, such as the Q-$Al_5Cu_2Mg_8Si$ phase (Fig. 1e,f). A comparison of Figures 1b and 1c reveals clear differences in the size and shape of the silicon particles. It is known that the shape change of Si eutectic morphology occurs in two stages: dissolution or fragmentation and granulation or spheroidization. Several researchers have argued that treating alloys with Sr before solution heat treatment facilitates the fragmentation of acicular silicon [24-26]. These different microstructural affect the mechanical properties, with a reduction in hardness. However, this reduction is offset by the greater dimensional stability of the precipitates, making the alloy less susceptible to shrinkage phenomena resulting from exposure to high operating temperatures. In particular, it was found that the microhardness of the substrate and the A357-T61 alloy electrode was 110 ± 3 HV and 58.2 ± 2 HV, respectively. While the microhardness of the substrate and C355-T61 alloy electrode was 100 ± 2 HV and 62.3 ± 2 HV.

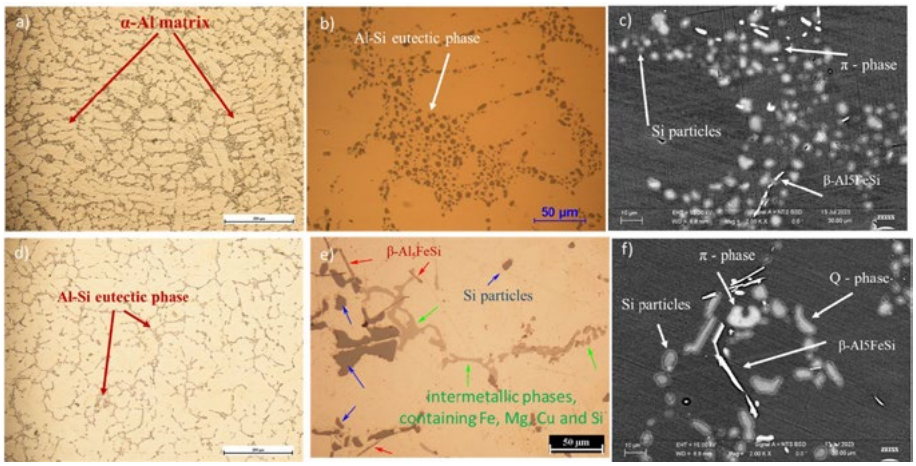

Fig.1 - Optical micrographs (OM) of the A357-T61 and C355-T61 substrates (base material), without chemical etching. a) OM showing dendrites of α-aluminum, b) OM of A357-T61 alloy showing the spheroidized eutectic Si particles and the intermetallic phases containing Fe, Mg, Cu and Si, c) SEM micrograph of A357-T61 alloy, d) OM of C355-T61 alloy showing an interdendritic network of mostly acicular Al-Si eutectic phase and secondary intermetallic phases and c) SEM micrograph of C355-T61 alloy.

APPEARANCE AND THICKNESS OF THE COATINGS

ESD is characterized by the ability to rapidly melt small amounts of electrode material using short pulses [14,15]. However, the amount of material involved in a layer deposition can vary significantly depending on the power discharge. Figure 2 a,b shows the cross-sectional macrograph (typical appearance) of coatings produced by the ESD process after 50 passes in aluminium alloy A357 using 33W (Fig. 2a) and in C355 using 37W (Fig. 2b). Interestingly, both deposits on A357 and C355 alloys exhibit similar widths, averaging around 1.6±1 mm. However, their thicknesses differ significantly depending on the discharge power used. Figure 3 shows a clear relationship between discharge power (P) and deposit thickness for both alloys. As the discharge power increases, the coating thickness also increases. Specifically, the C355 deposit thickness ranges from 12.2 μm (lowest power) to 169.2 μm (highest power). The A357 alloy deposits are even thicker, varying between 180.4 and 463 microns. This is due to the greater amount of material transferred at higher powers [15,27], leading to a faster growth rate (GR). Interestingly, A357 coatings exhibit a significantly greater increase in growth rate compared to C355 coatings, even at similar discharge powers. This is attributed to the higher hardness of the C355 electrode material, which limits the amount of material transferred during the process. These findings are consistent with previous research, including studies on NiCrAlY coatings by Cao et al. [28] and WE43 coatings by Renna G. et al. [29], which also highlight the influence of deposition parameters and pulse-spark energy (Es) on deposit thickness.

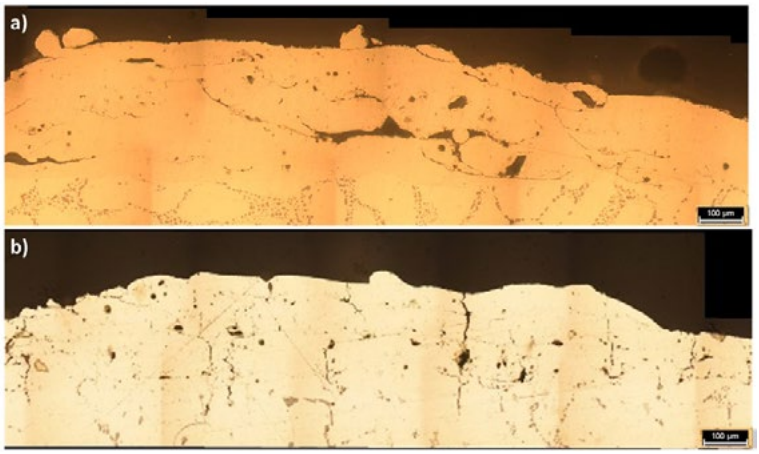

Fig.2 - OM of multiple-layer deposit products by ESD using a discharge power of: a) 33W for A357 alloy and b) 37W for C355 alloy; as can be seen, the deposits are affected by some defects.

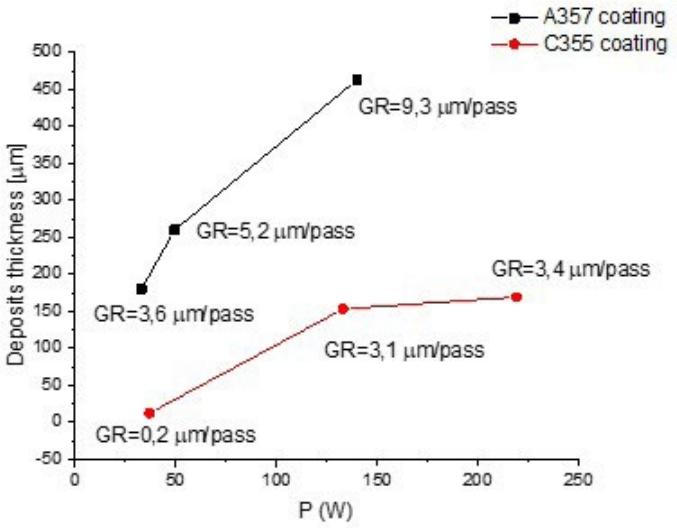

Fig.3 - Discharge power (P) vs. thickness for ESD deposits in A357 and C355 alloy.

Moreover, it was observed that the deposited coatings are affected by internal defects (see fig. 2 and fig. 4). These defects consist mainly of several voids, of different shapes-both spherical and laminar defects. These latter were likely caused by thermal stresses arising from the high-temperature gradients during the deposition process. Interestingly, these laminar shape defects can be found in two: perpendicular to the interface between the substrate and the coating and parallel to it (fig. 4). Spherical voids, typically ≤10 μm in size, are likely caused by entrapped gas during the deposition process. In addition, during the coating process, the melt may not be evenly distributed, leading to the formation of voids between adjacent deposited splats. These defects characterized by acicular-shaped voids are called bridging defects (fig. 4). The presence of these acicular voids (bridging defects) is detrimental to the strength of the coatings. They act as crack initiation sites, making the coatings more susceptible to failure under stress [14,15].

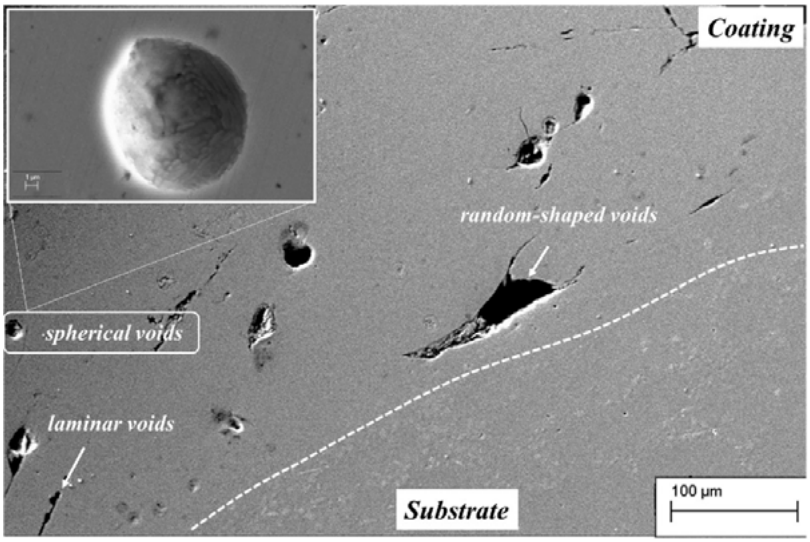

Fig.4 - SEM micrograph showing the typical voids of the coatings: small spherical voids, large, random-shaped voids, and laminar voids.

MICROSTRUCTURE OF THE COATINGS

Figure 5 shows the microstructure of A357 and C357 coatings deposited using ESD, viewed perpendicularly to the direction in which the layers were deposited (build direction). Figure 5a specifically provides a general overview of the initial appearance of the coatings, while Figure 5b illustrates typical microstructural features in the central region of the coatings. Regardless of the alloy used or electrical parameters set, the microstructures of the A357 and C355 coatings exhibit a distinct characteristic: thin, overlapping layers, forming a "layer-on-layer" structure (fig. 5b). This is attributed to the nature of the ESD process, where molten material is deposited layer by layer. Furthermore, the rapid cooling rates (10^5-10^6 °C/s) inherent to ESD lead to the formation of fine-grained microstructures within the coatings [15]. Interestingly, a closer examination using scanning electron microscopy reveals a cellular morphology within each layer (fig. 5 c,e). Additionally, at the interface between two adjacent layers, an equiaxial microstructure is observed (fig. 5 d,f). Rapid solidification theory helps explain the differences in the solidification structures observed. Kurz and Fisher [30] demonstrated that the ratio between the temperature gradient (G) and the solidification rate (V) is the key factor determining the final microstructure morphology. In other words, the relationship between the temperature gradient and the solidification rate affects the formation of microscopic structures during the solidification process. For example, a low solidification velocity and a high-temperature gradient may favor the formation of fine-grained structures, while opposite conditions may lead to the formation of coarser-grained structures [15].

Figure 6 a,b demonstrates the good adhesion between the ESD coatings and the substrates for both investigated alloys. Furthermore, there is no significant thermal impact on the substrates observed during the ESD process

(absence of heat-affected zone). Instead, Figures 6c and 6d show the presence of small Si eutectic particles partially or fully embedded within the coating, surrounded by a cellular structure. These particles likely originate from the substrate material, due to the intermixing of the BM and electrode materials during the ESD process. This mixing is believed to occur because the heat input involved in ESD is high enough to melt not only the electrode material but also a thin film of the substrate material.

It is noteworthy that, unlike A357 alloy coatings, the C355 alloy coatings interface was characterized by the presence of perpendicularly propagating cracks in the substrate (Figure 7a,b). This type of defect was also found in other ESD-treated aluminium alloys, such as alloy 2024. Both the morphology (shape and size) of the silicon particles and the morphology and distribution (arrangement) of the secondary phases (Fe-containing intermetallics) are believed to significantly influence the formation of cracks at the interface. Therefore, the amount of eutectic structure can influence the coating quality. In general, during the deposition process, the coarse eutectic structure of silicon can negatively impact the deposition process. These large silicon particles can hinder the material's ability to expand uniformly (volumetric expansion) during solidification, leading to localized areas of stress and crack formation [22].

In contrast, substrates with finer eutectic structures, like A357, allow an engulfment mechanism of silicon particles within the first deposited layers, resulting in a stronger and more uniform bond between the coating and the substrate. Furthermore, the presence of acicular (needle-shaped) intermetallic phases, such as β-phase, within the substrate adds another aspect of complexity. These intermetallics, due to their brittle nature, can act as stress concentrators, making them susceptible to fracture even before eutectic silicon. In addition, their morphology acts as stress concentration points, further contributing to the formation of microfractures that propagate at the interface between the intermetallics and the surrounding matrix.

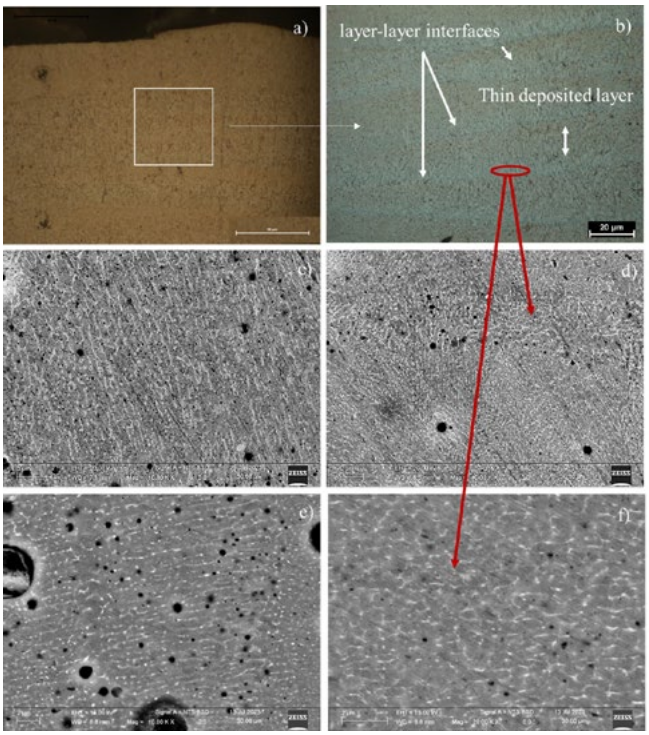

Fig.5 - Microstructural analysis of the coatings: a) OM representing the typical aspect of cross-section coatings, b) OM of the central region of the coating cross-section after chemical etching showing the typical layer-by-layer microstructure, c) SEM micrograph showing the cell type morphology within each layer for the coating in A357 alloy, d) SEM micrograph showing the equiaxed type morphology within each layer-layer interface for the coating in A357 alloy and c) SEM micrograph showing the cell type morphology within each layer for the coating in C355 alloy, d) SEM micrograph showing the equiaxed type morphology within each layer-layer interface for the coating in C355 alloy.

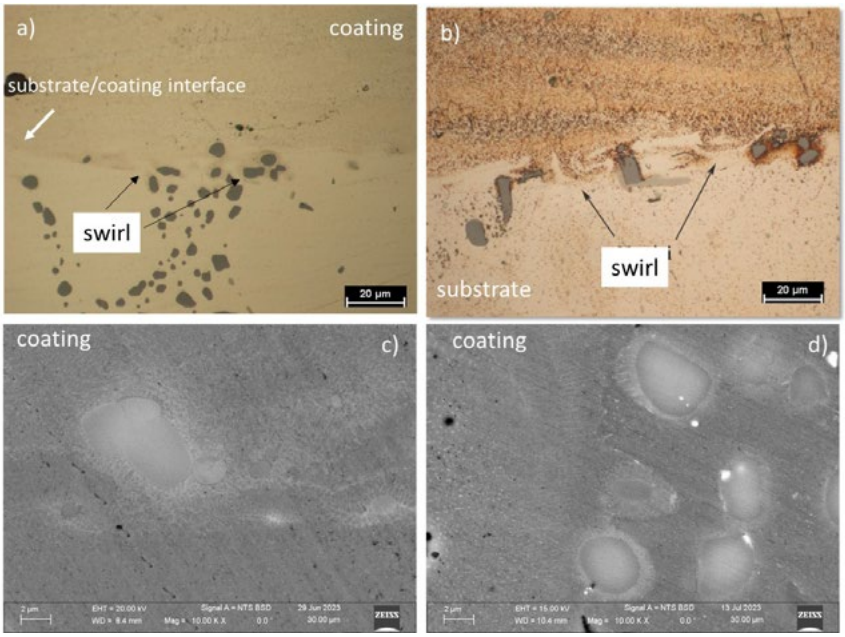

Fig.6 - Microstructural analysis of the substrate/coating interface: a) OM of the interface region for A357 coating, b) OM of the region for the C355 coating and c, d) SEM micrographs of the interface region for the coating in A357 and C355 alloy, respectively.

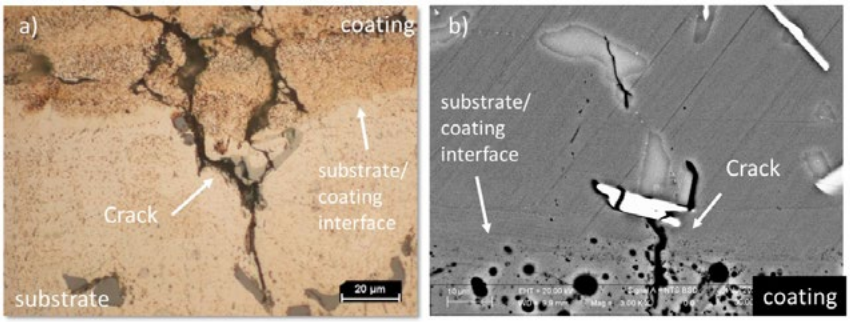

Fig.7 - Coatings in C355 alloy: a) OM and b) SEM micrograph of the coating/substrate interface showing the crack that propagates in the substrate along intermetallic phases.

DEFECT ANALYSIS AND COATING HARDNESS.

Table 3 presents the average crack length and occurrence frequency for the C355 samples processed at the three different discharge powers. The occurrence frequency is calculated as the ratio of the number of observed cracks to the total length of the examined interface. Interestingly, the occurrence frequency at the interface remains consistent regardless of the applied power in the ESD process. However, the average crack length increases with increasing power. This phenomenon can be explained by considering two key factors: the location of crack initiation remains consistent across all three depositions due to the inherent characteristic microstructural of the substrate (distribution and morphology of the secondary phases). Secondly, as the applied power increases, the heat input to the substrate also increases. This additional heat contributes to the growth of the triggered cracks, leading to an increase in their average length [14].

To evaluate the coatings' resistance and durability and to indicate the amount of defects present in the coatings, microhardness and percentage defects measurements were performed. The percentage area fraction of defects was calculated as the ratio of the area of the voids present to the area of the examined coating.

Figure 8 illustrates the average microhardness and percentage area fraction of defects across the cross-section of A357 and C355 samples, as a function of the applied power. Both A357 and C355 coatings exhibit a

limited overall defect percentage, with A357 below 4% and C355 below 7% of the total surface area. Notably, in A357 and C355 coatings, the percentage of defect area shows a decreasing trend with increasing power. The decrease is much more pronounced for the C355 alloy. The authors attribute the observed decrease in defects with increasing power to a reduction in laminar defects. These defects are typically associated with the ESD process due to its high energy density and low heat input, leading to both parallel ("delamination cracks") and perpendicular cracks at the interface [20,31]. Delamination cracks are primarily linked to poor mixing between the electrode material and previously deposited layers, while perpendicular cracks are generally attributed to high thermal gradients [20,31]. Higher power settings lead to the melting of larger volumes of electrode and substrate material, promoting better mixing and adhesion between them. This potentially reduces delamination cracks. Additionally, the increased power raises the temperature of the substrate and existing layers, minimizing thermal gradients and further reducing the risk of crack initiation.

Despite the expectation of higher microhardness due to their finer microstructure, the coatings exhibit lower hardness compared to the substrate. This is likely due to the widespread presence of defects. Supporting this, the lowest hardness for C355 coincides with the highest defectivity observed at the minimum power setting (at minimum power).

Tab.4 - Average crack length and the ratio between the cracks number and interface length examined (occurrence frequency) for the coatings in C355 alloy.

Samples	P [W]	Average crack length (μm)	N_{tot}/mm
C1	37	20,6	4
C2	133,2	28,2	3
C3	219,4	33,4	3

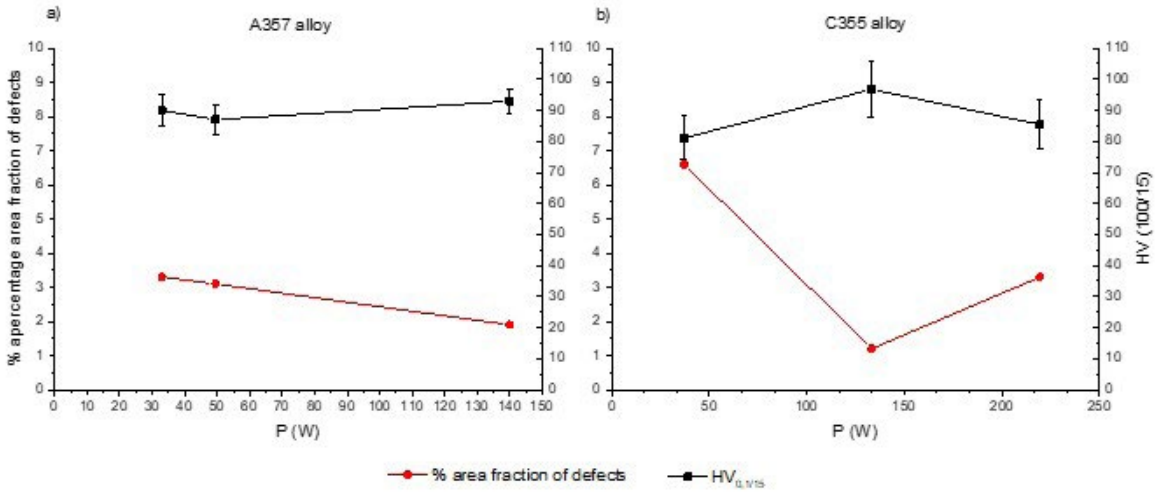

Fig.8 - Microhardness and percentage area fraction of defects as a function of discharge power (P) for a) A357 alloy and b) C355 alloy.

CONCLUSIONS

The study and comparison of coatings in A357 and C355 prepared on the as-cast substrates in homologous material by ESD produced the following results:

- The microstructural analysis shows that a nanostructured solidification structure for A357 and C355 coatings can be commonly achieved by this technique. However, the powers used to deposit both alloys do not result in changes in the microstructure. All coatings share a common microstructure: overlapping layers with distinct interfaces.
- The morphology (shape and size) and distribution of silicon (Si) particles and secondary phases within the substrate significantly influence the formation of the coatings. This is because these features can affect the formation of defects at the interface between the substrate and the coating.
- Both coatings exhibited defects of various shapes, including laminar, spherical, and random. Unlike the A357 coatings, C355 coatings exhibit a new type of defect: cracks propagating perpendicularly (at right angles) into the substrate from the coating interface.
- The number of cracks at the interface remains constant regardless of the applied power during the ESD process. However, the average crack length increases with increasing power. This suggests that the crack initiation points, likely determined by the substrate's microstructure, remain consistent across the three depositions.
- Despite variations in discharge power, the microhardness of A357 and C355 coatings remains lower than the substrate, primarily influenced by the presence of internal defects.
- Generally, higher applied power, and current density, promote the growth of coating.

REFERENCES

[1] W.S. Miller, L. Zhuang, J. Bottema, A.J. Wittebrood, P. De Smet, A. Haszler, A. Vieregge, Recent development in aluminium alloys for the automotive industry, Mater. Sci. Eng. A 80 (2000) 37–49.
[2] ASM Handbook, 18, Friction, Lubrication, and Wear Technology, S.D. Henry (Ed.), ASM International (1992) 553–562, 786–794
[3] M. Elmadagli, T. Perry, A.T. Alpas, A parametric study of the relationship between microstructure and wear resistance of Al–Si alloys, Wear 262 (2007) 79–92
[4] Khaled Salem Alhawari, Mohd Zaidi Omar, Saziana Samat, Ahmad Muhammad Aziz. Effect of magnesium addition consolidated by the thixoforming process on the wear properties of A319 alloy, The International Journal of Advanced Manufacturing Technology https://doi.org/10.1007/s00170-024-13288-2
[5] N.D. Alexopoulos, Sp.G. Pantelakis, Quality evaluation of A357 cast aluminum alloy specimens subjected to different artificial aging treatment. Materials and Design 25 (2004) 419–430
[6] I.J. Polmear, Light Alloys: Metallurgy of the Light Metals, Butterworth Heinemann, 1995
[7] Davis, J.R. ASM specialty handbook: Aluminum and Aluminum Alloy. ASM International; 1993.
[8] Engler-pinto Jr, C.C., et al., A comparative investigation on the high temperature fatigue of three cast aluminum alloys. SAE Transactions, 2004. Paper # 2004-01-1029.
[9] G. Mrówka-Nowotnik, J. Sieniawski Microstructure and mechanical properties of C355.0 cast aluminium alloy, Archives of the material science and engeniring Volume 47, Issue 2, February 2011, Pages 85-94
[10] Z. Li, A.M. Samuel, F.H. Samuel, C. Ravindran, S. Valtierra, H.W. Doty, Parameters controlling the performance of AA319-type alloys Part I. Tensile properties, Materials Science and Engineering 367 (2004) 96-110.
[11] Z. Li, A.M. Samuel, C. Rayindran, S. Valtierra, H.W. Doty, Parameters controlling the performance of AA319-type alloys: Part II. Impact properties and fractography, Materials Science and Engineering 367 (2004) 111-122.
[12] F. King, Aluminium and its alloys, John Willey and Sons, New York, Chichester, Brisbane, Toronto, 1987.
[13] Victor Verbitchi, Cristian Ciuca, Radu Cojocaru, Electro-Spark Coating with Special Materials. Nonconventional Technologies Review – no. 1/201
[14] Paola Leo, Gilda Renna and Giuseppe Casalino, Study of the Direct Metal Deposition of AA2024 by ElectroSpark for Coating and Reparation Scopes Appl. Sci. 2017, 7, 945
[15] Barile, C.; Casavola, C.; Pappalettera, G.; Renna, G. Advancements in Electrospark Deposition (ESD) Technique: A Short Review. Coatings 2022, 12, 1536. https://doi.org/10.3390/coatings12101536ù
[16] Wang, P.Z.; Pan, G.S.; Zhou, Y.; Qu, J.X.; Shao, H.S. Accelerated Electrospark Deposition and the Wear Behavior of Coatings. J. Mater. Eng. Perform. 1997, 6, 780–784.

[17] Xie, Y.J.; Wang, M.C. Microstructural morphology of electrospark deposition layer of a high gamma prime superalloy. Surf. Coat. Technol. 2006, 201, 691–698
[18] Liu, D.Y.; Gao, W.; Li, Z.W.; Zhang, H.F.; Hu, Z.Q. Electro-spark Deposition of Fe-based Amorphous Alloy Coatings. Mater. Lett. 2007, 61, 165–167.
[19] P. Cavaliere, E. Cerri, P. Leo, Journal of Materials Science, volume 39, issue 5, year 2004, pp. 1653 – 1658
[20] P. Leo, G. Renna, Rivestimenti via Electrospark Deposition in lega A357: microstruttura e difettosità. La Metallurgia Italiana - n. 9 2019
[21] Lorella Ceschini, Alessandro Morri, Andrea Morri, Stefania Toschi, Sten Johansson, Salem Seifeddin Effect of microstructure and overaging on the tensile behavior at room and elevated temperature of C355-T6 cast aluminum alloy. Materials & Design 83 (2015) 626–634
[22] Davis, J.R. ASM specialty handbook: Aluminum and Aluminum Alloy. ASM International; 1993
[23] L.F. Mondolfo, Aluminium Alloys: Structure and Properties, London-Boston, Butterworths, 1976.
[24] B. Parker, "Quantitative evaluation of the microstructure of a strontium-modified Al-Si-Mg alloy following prolonged solution treatment," Metals Forum, vol. 5, no. 1, pp. 48–53, 1982.
[25] F. N. Rhines and M. Aballe, "Growth of silicon particles in an aluminum matrix," Metallurgical Transactions A, vol. 17, no. 12, pp. 2139–2152, 1986.
[26] Mohamed Ibrahim, Mohamed Abdelaziz, Agnes Samuel, Herbert Doty, and Fawzy Samuel Spheroidization and Coarsening of Eutectic Si Particles in Al-Si-Based Alloys Advances in Materials Science and Engineering Volume 2021, Article ID 6678280, 16 pages https://doi.org/10.1155/2021/6678280
[27] Heard, D.W.; Brochu, M. Development of a nanostructure microstructure in the Al–Ni system using the electrospark deposition process. J. Mater. Process. Technol. 2010, 210, 892–898
[28] Cao, G.J.; Wang, Y.Y.; Tang, G.Z. Properties of NiCrAlY coatings fabricated on superalloy GH4169 by electrospark deposition. Int. J. Adv. Manuf. Technol. 2018, 96, 1787–1793.
[29] Gilda, R.; Paola, L.; Caterina, C. Effect of ElectroSpark Process Parameters on the WE43 Magnesium Alloy Deposition Quality. Appl. Sci. 2019, 9, 4383.
[30] W. Kurz D. J. Fisher, Fundamentals of Solidification, Trans Tech Publications, Switzerland 1998
[31] M.H. Staia, A. Fragiel, M. Cruz, E. Carrasquero, B. Campillo, R. Perez, M. Constantino , T.S. Sudarshan, Wear 251 (2001) 1051– 1060

TORNA ALL'INDICE >